Development of Marinized Pt-Modified MCrAlX Coatings with Improved Hot Corrosion and Oxidation Resistance Synthesized via a Low-Cost Electrodeposition Process

Final Report

Final Report: Grant N00014-14-1-0341

Submitted to:
Dr. David Shifler
Office of Naval Research

By
Ying Zhang
Department of Mechanical Engineering
Tennessee Technological University
Cookeville, TN 38505-0001

January 22, 2019

REPORT DOCUMENTATION PAGE

Form Approved
OMB No. 0704-0188

PLEASE DO NOT RETURN YOUR FORM TO THE ABOVE ORGANIZATION.

1. REPORT DATE *(DD-MM-YYYY)*	2. REPORT TYPE	3. DATES COVERED *(From - To)*
22-01-2019	Final	03/14/2014 - 12/31/ 2018

4. TITLE AND SUBTITLE
Development of Marinized Pt-Modified MCrAlX Coatings with Improved Hot Corrosion and Oxidation Resistance Synthesized via a Low-Cost Electrodeposition Process

5a. CONTRACT NUMBER

5b. GRANT NUMBER
N00014-14-1-0341

5c. PROGRAM ELEMENT NUMBER

6. AUTHOR(S)
Zhang, Ying

5d. PROJECT NUMBER
14PR04963

5e. TASK NUMBER

5f. WORK UNIT NUMBER
332

7. PERFORMING ORGANIZATION NAME(S) AND ADDRESS(ES)
Tennessee Tech University
PO Box 5036
Cookeville, TN 38505-0001

8. PERFORMING ORGANIZATION REPORT NUMBER

9. SPONSORING/MONITORING AGENCY NAME(S) AND ADDRESS(ES)
Office of Naval Research
875 North Randolph Street
Arlington, VA 22203-1995

10. SPONSOR/MONITOR'S ACRONYM(S)
ONR

11. SPONSOR/MONITOR'S REPORT NUMBER(S)

12. DISTRIBUTION/AVAILABILITY STATEMENT
Approved for public release: distribution unlimited.

13. SUPPLEMENTARY NOTES

14. ABSTRACT
The project aimed to develop Pt-modified MCrAlX coatings (where X = Si+Y+Hf, etc.) for the hot-section components in Navy gas turbine engines utilizing a low-cost electrodeposition process. A rotating barrel system was established to deposit NiCo-CrAlX coatings with uniform particle incorporation on various specimen geometries. Post-deposition heat treatment promoted interdiffusion between the CrAlX particles and Ni/Co matrix, leading to the formation of β, γ' and γ phases. The effects of heat treatment parameters were investigated. A Dean rig was built for hot corrosion screening tests. The cyclic oxidation behavior of electro-codeposited NiCoCrAlY coatings on Ni-based superalloys was evaluated at 1000 and 1100°C. Preliminary Type I hot corrosion testing was conducted in the Dean rig with flowing O2 + 0.1% SO2 gas. Compared to the NiAl coatings made by non-contact pack cementation, the NiCoCrAlY coatings had better overall resistance to both cyclic oxidation and hot corrosion and also exhibited superior compatibility with the superalloy substrates. The mechanical properties of model NiCoCrAlY alloys were also evaluated. Furthermore, selected NiCoCrAlY coatings were successfully applied to the burner rig pins for further evaluation.

15. SUBJECT TERMS
electro-codeposition, rotating barrel, CrAlY particle incorporation, post-deposition heat treatment, oxidation, hot corrosion

16. SECURITY CLASSIFICATION OF:			17. LIMITATION OF ABSTRACT	18. NUMBER OF PAGES	19a. NAME OF RESPONSIBLE PERSON
a. REPORT	b. ABSTRACT	c. THIS PAGE		21	YING ZHANG
					19b. TELEPHONE NUMBER *(Include area code)* 931-372-3969

Reset

Standard Form 298 (Rev. 8/98)
Prescribed by ANSI Std. Z39.18
Adobe Professional 7.0

Development of Marinized Pt-Modified MCrAlX Coatings with Improved Hot Corrosion and Oxidation Resistance Synthesized via a Low-Cost Electrodeposition Process

Final Report: Grant N00014-14-1-0341

1. Technical Objectives

Increasing the operational capabilities of the U.S. Navy surface ship gas turbine engines will require higher operating temperatures and change the associated operating environment to one where high-temperature hot corrosion (HTHC), low-temperature hot corrosion (LTHC), and oxidation will be prevalent.[1] It is also expected that hot-section propulsion materials will experience frequent cycles between different temperature regimes and consequently more severe thermomechanical fatigue (TMF). Marinized coatings with improved corrosion and oxidation resistance that can function in this environment are needed to protect engine hot-section components. The project aims to develop marinized MCrAlX coatings (where X = Si+Y+Hf, etc.) for the hot-section components in Navy gas turbine engines utilizing a low-cost electrodeposition process. The coating development will focus on improving the resistance against various degradation mechanisms including LTHC, HTHC, oxidation, and TMF. Coating composition, phase constituents and processing parameters will be optimized in order to achieve the required overall coating performance.

The technical objectives of this research effort included:

(1) Development of electrodeposited MCrAlX coatings and optimization of post-deposition heat-treating parameters

(2) Evaluation of the cyclic oxidation performance of MCrAlX coatings at 1000 and 1100°C

(3) Evaluation of the hot corrosion performance of MCrAlX coatings

(4) Investigation of the mechanical properties of MCrAlY model alloys

(5) Development of MCrAlX coatings on burner rig pins

2. Technical Approach

2.1. Electro-codeposition experiments

Substrates were made from nickel-based alloys including Ni 200 (>99.0 Ni, with 0.25Cu-0.40Fe-0.35Mn-0.15C-0.35Si-0.01S max., in wt%), directionally-solidified Ni-based superalloy René 80 provided by GE Aviation (59.7Ni-3.0Al-14.1Cr-9.7Co-4.3W-4.0Mo-5.0Ti-0.18C in wt.% and 130B-200Zr-7S in ppmw), and single-crystal superalloy CMSX-4 provided by Rolls-Royce Corporation (60.7Ni-5.9Al-6.3Cr-9.6Co-6.5W-0.6Mo-2.9Re-6.5Ta-1.0Ti in wt.% and 1100Hf-17C-1S in ppmw). The specimens were ground to #600 grit using SiC grinding papers, grit blasted with #220 Al_2O_3 grit, followed by ultrasonicalcleaning in hot water and acetone. Two laboratory ball-milled CrAlY(Ta) alloy powders and two commercial gas-atomized CrAlY powders purchased from Sandvik were used in the electro-codeposition experiments. The chemical compositions and other characteristics of the four powders are given in Table 1. It should be noted that unless specifically noted, the ball-milled CrAlY powder was used in the electro-codeposition.

Three configurations were initially used in the electro-codeposition process, i.e., the vertical and horizontal arrangements in a 1000-mL beaker, and a rotating barrel.[2,3] Most of the testing

specimens were later coated in the rotating barrel system (Fig. 1) due to its capability of depositing coating on the entire specimen surface.[4,5] Watts nickel/cobalt plating solution (Table 2) was used and the nickel anode was placed outside of the barrel along with a mechanical stirrer and the heating coil. The specimens were plated at 50°C and the plating solution pH was maintained at around 3.5. The typical plating current density was 20 mA/cm^2, and the CrAlY particle concentration in the plating solution was 20 g/L for all coupon samples.

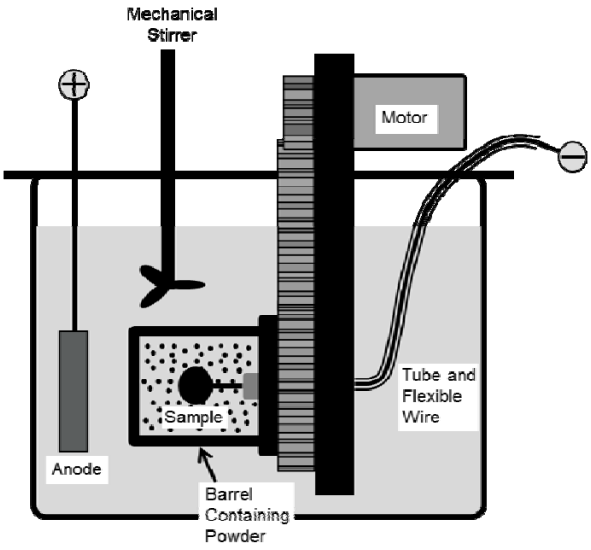

Fig. 1. Schematic of the barrel system.

Table 1. Compositions (wt.%) and properties of the alloy powders used in the electro-codeposition experiments.

	Cr	Al	Y	Ta	D_{50} (μm)	Shape	Density (g/cm^3)
Ball-milled CrAlY (TTU)	61.3	37	1.7	—	5.6	Irregular	4.5
Ball-milled CrAlYTa (TTU)	60.6	25.3	1.5	12.6	—	Irregular	5.5
Atomized CrAlY (Sandvik)	67.8	29.7	1.65	—	4.7	Spherical	5.0
Atomized CrAlY (Sandvik)	68.0	29.8	2.0	—	10.1	Spherical	5.0

Table 2. The composition of the plating bath and typical operating conditions

Plating solution with particles	**Operating conditions**
$NiSO_4 \cdot 6H_2O$: 212.1 g/L	Current density: 20 mA/cm^2
$NiCl_2 \cdot 6H_2O$: 44.5 g/L	Barrel speed: 7 rpm
$CoSO_4 \cdot 7H_2O$: 12.3 g/L	Bath temperature: 50°C
H_3BO_3: 32.2 g/L	pH value: 3.5
$CH_3(CH_2)_{11}OSO_3Na$: 0.2 g/L	
CrAlY particles: 20 g/L	

2.2. Oxidation and hot corrosion testing

Automated cyclic oxidation tests were conducted on uncoated and coated alloys at 1000 and 1100 °C in dry oxygen at Oak Ridge National Laboratory (ORNL).[6] Each cycle consisted of a 1-h exposure at temperature followed by a 10-min cooling period in ambient air. Specimens were weighed after every 20 or 50 cycles. For the 1000 °C test, uncoated and coated René 80 specimens were included, whereas coatings on both René 80 and CMSX-4 were evaluated at 1100 °C. The NiCoCrAlY coatings evaluated in the oxidation tests were either ~50 or 100 μm thick.

Preliminary hot corrosion tests were also carried out in a modified Dean rig,[7] which consisted of a hot zone where an Na_2SO_4 reservoir was heated above its melting point and a cooler zone downstream where the evaporated salt condensed onto the test specimens. The testing procedure was in accordance with what was previously reported by Deodeshmukh and Gleeson.[8] The specimens were placed in the "cooler zone" at 900 °C for Type I corrosion testing. A carrier gas of O_2 + 0.1% SO_2 was passed through a platinum-plated nickel foam catalyst to form an equilibrium amount of SO_3 in the atmosphere. The gas flow rate was ~22 ml/min, which was equivalent to a linear velocity of 0.25 mm/s. Prior to hot corrosion testing, 2-3 mg/cm^2 of Na_2SO_4 salt was sprayed on the specimen at ~200 °C using an airbrush. After every 20 h of exposure, the specimens were cooled to room temperature, weighed, and then re-sprayed with 2-3 mg/cm^2 of salt. Specimens were tested for up to 200 h under Type I hot corrosion condition.

2.3. Mechanical testing

To understand the effect of the coating composition (particularly the Al and Cr levels) on its mechanical properties, MCrAlY model alloys were evaluated in tensile testing in a temperature range of 20-800°C. The model alloys were fabricated at TTU via arc melting and drop casting. Homogenization annealing was conducted for 24h at 1000°C (Alloys 1-7) or 4h at 1300°C (Alloys 8-9). Miniature dog-bone specimens, 25.4 mm long and 2 mm × 1 mm in gage section, were prepared by electrical discharge machining and subsequent polishing to a 600-grit finish. Tensile tests were carried out at ORNL with an Instron electro-mechanical machine at four different temperatures, including room temperature (20°C), 400, 600, and 800°C, with a strain rate of 10^{-3} s^{-1}. The strain was calculated from the crosshead displacement. Microhardness (Vickers) testing was also carried out on the polished cross sections using a load of 200-500 gf.

2.4. Microstructural characterization

Before and after testing, specimens were examined by visual inspection, optical microscopy, scanning electron microscopy (SEM) equipped with energy dispersive spectroscopy (EDS), and X-ray diffraction (XRD). Prior to metallographic sectioning, specimens (except the specimens after hot corrosion testing) were Cu-plated to improve edge retention. To determine the volume fraction of the incorporated CrAlY particles in as-deposited coatings, multiple backscattered electron images were taken from different locations along the coating cross-section, which were then processed using the ImageJ software.[9] The brightness and contrast of the image were adjusted by setting a proper threshold such that the particles were separated from the background. The area fraction of the CrAlY particles was determined, which was assumed equivalent to its volume fraction.

For corrosion-tested specimens, use of water-based products was avoided during metallographic sample preparation to preserve the water-soluble corrosion product on the surface. Corrosion

penetration depth was measured using the optical microscope equipped with Nikon NIS Elements software. The original specimen thickness was measured at three locations and the corrosion depth was determined in the form of maximum and average internal attacks. The average internal attack was calculated by subtracting the remaining unaffected metal from the original specimen thickness, which included all oxidation and corrosion species that attacked the metal, but excluded the sulfidation zone. A minimum of 40 measurements were taken on the cross-section of each corrosion-tested specimen. Minitab software was utilized to analyze the corrosion data.

3. Results and Discussion

3.1. Development of electrodeposited MCrAlX coatings and optimization of post-deposition heat-treating parameters

The cross-section of the as-deposited (Ni,Co)-CrAlY composite coating shown in Fig. 2. The coating was approximately 50 μm thick after 2-h plating, and 35-40 vol.% of CrAlY particles were uniformly distributed in the (Ni,Co) matrix.

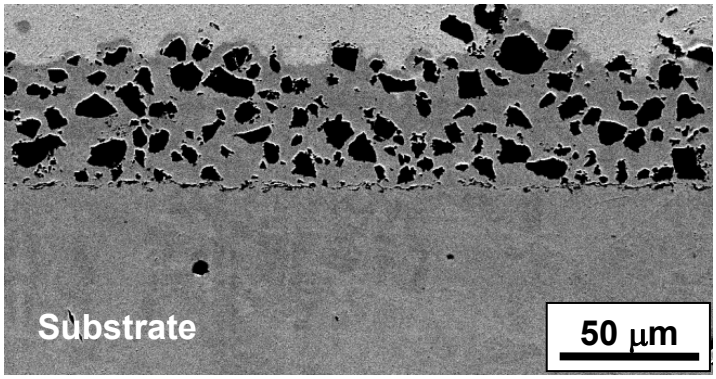

Fig. 2. SEM cross-section of the as-deposited (Ni,Co)-CrAlY composite coating.

The René 80 specimens coated with the (Ni,Co)-CrAlY composite coating were heat-treated for 2h in either vacuum or Ar at three different temperatures (i.e., 1000, 1100, and 1200°C). One coated specimen was sectioned into two halves; one half was heat-treated in vacuum and the other in Ar at the same temperature. Figure 3 provides a schematic illustration of the coating microstructural evolution during the heat treatment. Interdiffusion between the CrAlY particles and the (Ni,Co) matrix led to the formation of a variety of phases, such as β-NiAl, γ'-Ni_3Al and γ-Ni, depending on the heat-treating temperature. In general, the β phase outlined the shape of the original CrAlY particles, surrounding an area of γ + γ' or γ + γ' + β. The original γ-(Ni,Co) matrix changed to γ + γ' after heat treatment. Voids were also observed at the interface of β and the γ + γ' matrix.[10]

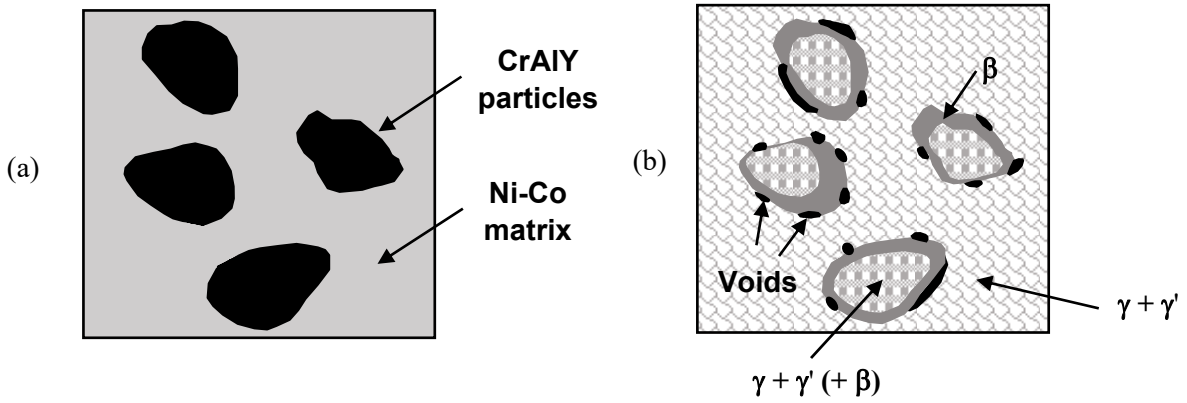

Fig. 3. Schematic illustration of the coating microstructure before (a) and after (b) heat treatment.

The EDS concentration depth profiles of the major elements in the electrodeposited NiCoCrAlY coatings after different heat treatments are presented in Fig. 4. The as-deposited coating surface contained 18-21% Al, 23-28% Cr, and 10-12% Co (in wt.%). After heat treatment, the surface Al content decreased to 8-14%, as a result of the interdiffusion between the coating and the superalloy substrate. However, the reduction of Cr near the coating surface was much more significant, particularly for the coatings heat-treated in vacuum at 1100-1200°C, which was attributed to the evaporation of volatile Cr from the coating surface at elevated temperatures, as also reported for the MCrAlY coatings made by thermal spraying and electron-beam physical vapor deposition.[11,12] After 2h at 1200°C in vacuum, the Cr content of the NiCoCrAlY coating dropped to only 3% on the surface, whereas the Cr level remained 14% on the surface for the coating heat-treated in Ar. In addition, during heat treatment at 1200°C (regardless of the environment), Ti diffused from the René 80 substrate into the coating layer, and up to 2 wt.% of Ti was detected at the coating surface.[13] In the coating layer away from the surface, the overall coating compositions were Ni-(14-18)Co-(11-15)Cr-(8-10)Al (wt.%). These results suggest that the post-deposition heat treatment is preferable to be conducted at temperatures <1100°C in Ar to minimize Cr evaporation as well as to prevent diffusion of Ti from the superalloy substrate to the coating surface.

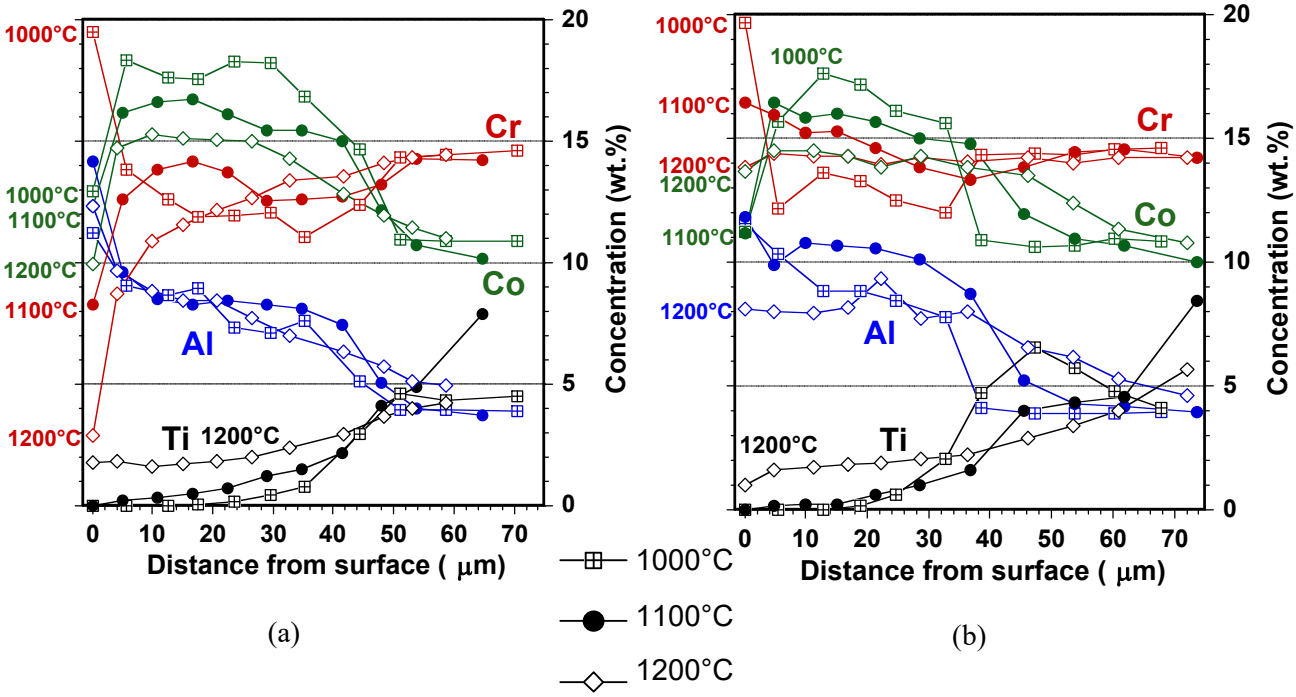

Fig. 4. EDS concentration profiles of the major elements in the NiCoCrAlY coatings on René 80 after heat treatment in vacuum (a) and Ar (b).

3.2. Evaluation of the cyclic oxidation performance of MCrAlX coatings at 1000 and 1100°C

Figure 5 shows the specimen mass change data for bare and coated René 80 specimens during the cyclic oxidation test at 1000°C. A diffusion NiAl coating made by non-contact pack aluminization was included for comparison.[14] Uncoated René 80 experienced mass loss beginning at 250 cycles and continued to lose mass throughout the duration of the remaining test (−64.8 mg/cm^2 after 550 cycles), indicating very poor oxide-scale adherence. If failure is defined

as zero crossover,[15] i.e., when the sample weight after a test interval is less than or equal to the initial weight, the cyclic oxidation life of the bare alloy was ~250 cycles at 1000°C. The NiAl coating and the majority of the electro-codeposited MCrAlX coatings (50-100 μm thick) showed stable low mass gains (e.g., <2.5 mg/cm^2) up to 1000 cycles at 1000°C and did not reach the zero crossover when the test was stopped. However, continuous mass losses occurred for several 50-μm MCrAlX coatings (Fig. 5), while no obvious scale spallation was observed on the majority of the specimen surface.

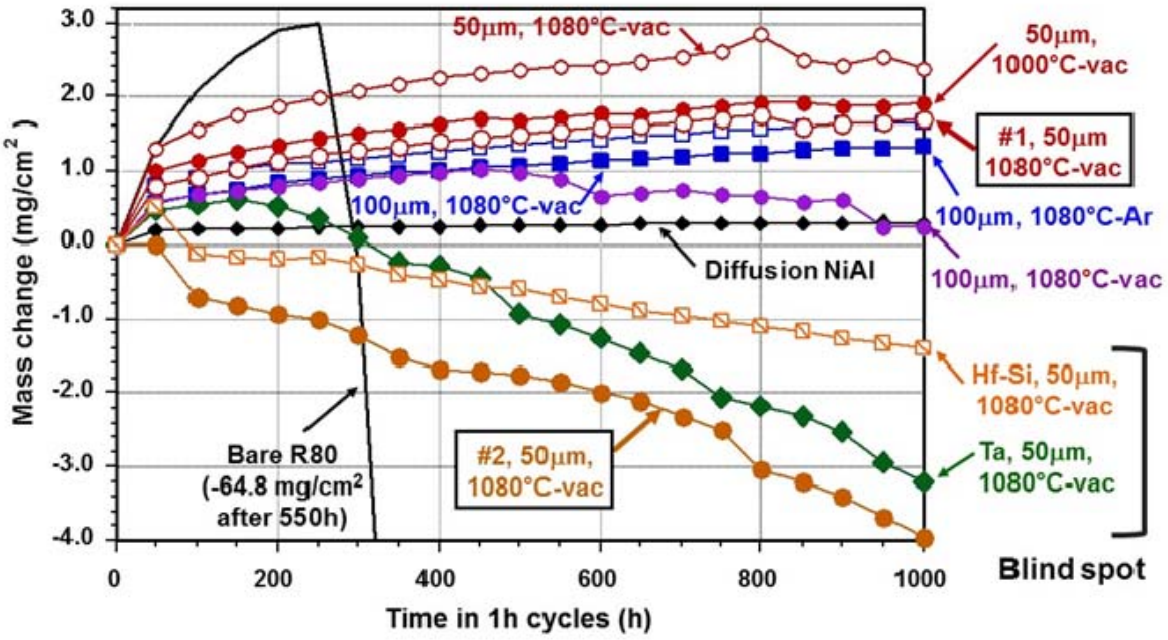

Fig. 5. Mass change of bare and coated René 80 specimens in the cyclic oxidation test at 1000°C.

The surface and cross-section of two representative samples (#1 with a very low mass gain and #2 with a continuous mass loss) are presented in Figs. 6 and 7, respectively. For the coatings with low mass gains such as Specimen #1, a thin adherent scale (mainly alumina) was formed after 1000, 1h cycles at 1000°C. For the specimens showed continuous mass losses (e.g., Specimen #2), while adherent oxide scales were observed on the majority of sample surface (Figs. 7a and c), an area on the specimen bottom edge exhibited severe scale spallation (Fig. 7b) where large oxide nodules (Fig. 7d) and thicker oxide scales (Fig. 7e) were observed. Ti-rich precipitates were also noticed underneath the oxide scale in the spallation area (Fig. 7e). Due to the specific specimen alignment in the rotating barrel during electrodeposition, a "blind spot" could form on the specimen edge along the center axis around which the specimen was rotating (Fig. 7a). In this particular area, the CrAlX particle incorporation was very low, resulting in extremely low Al and Cr contents and poor oxidation resistance in this area. Corrections of sample alignment in the barrel were then made to reduce the blind spot size on the specimen.

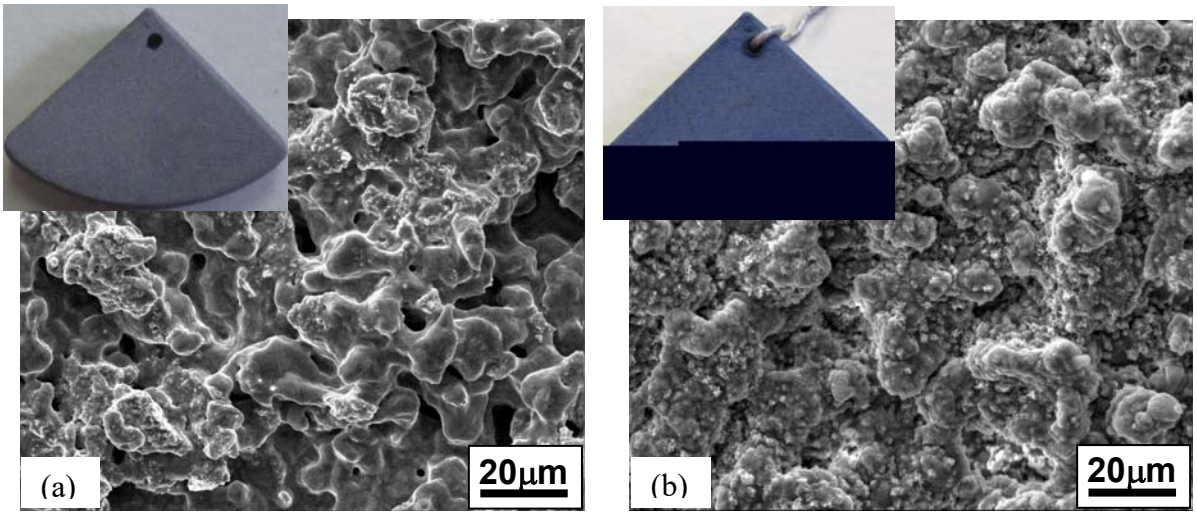

Fig. 6. Specimen #1 before and after oxidation: (a) surface before oxidation, (b) surface after oxidation, and (c) SEM cross-sectional image after oxidation.

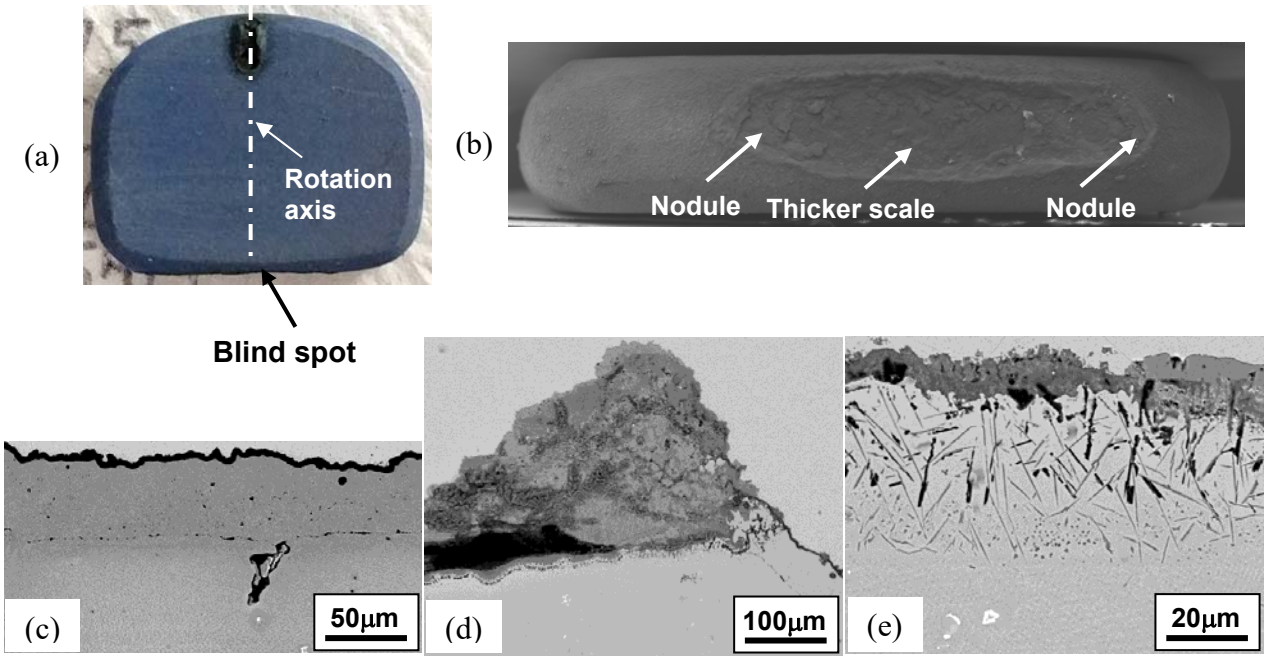

Fig. 7. Specimen #2 (with the "blind spot") after oxidation: (a) overall specimen appearance, (b) spallation on the "blind spot", (c) SEM cross-sectional image of the areas where oxide scales were adherent, (d) large oxide nodules formed in the "blind spot" area, and (e) thicker oxide scale and precipitates underneath the scale formed in the "blind spot" area.

Figure 8 shows the mass change data of bare and coated specimens in 1100°C testing. At this testing temperature, the uncoated René 80 reached the zero crossover point after only 70 h and showed a mass loss of −128.3 mg/cm^2 when the specimen was removed after 250 h. The uncoated CMSX-4 exhibited much better oxidation resistance with a crossover time of 330 h and −11.8 mg/cm^2 mass loss after 750 h. The NiCoCrAlY-coated René 80 specimens reached the zero crossover at 500-750 h; the coating heat-treated in Ar had a lower mass gain and a longer lifetime. The two NiCoCrAlY-coated CMSX-4 specimens exhibited longer crossover times, 1050-1100 h. The NiAl-coated René 80 exhibited ~1000 h crossover time, which also showed the lowest mass gain among all tested coating samples.

.

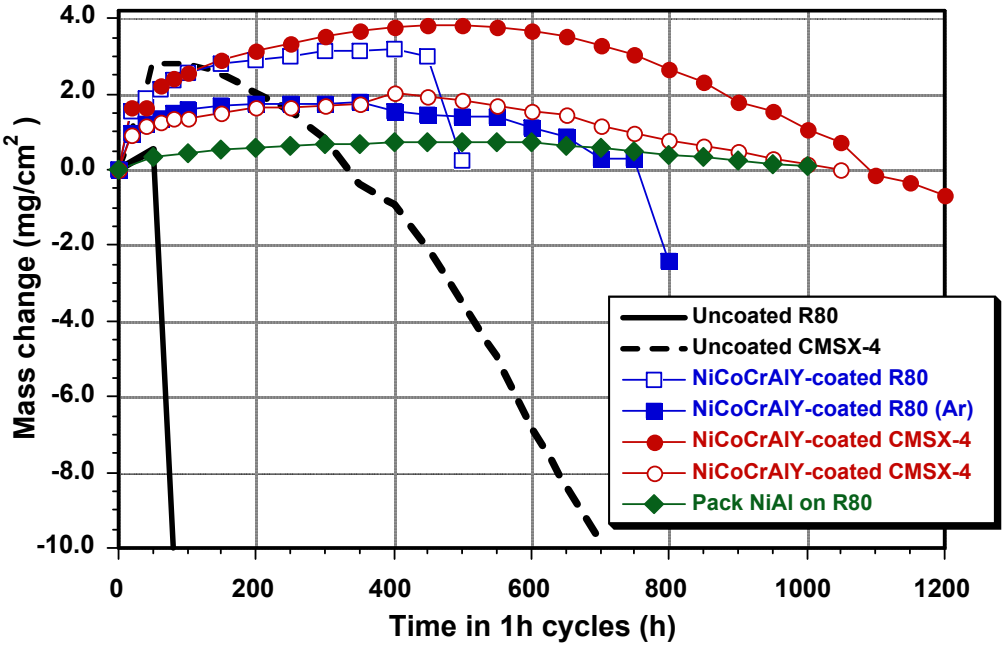

Fig. 8. Specimen mass changes during 1-h cycles at 1100 °C.

Comparison of the coating surface morphology before and after oxidation (Fig. 9) indicates that the change in surface morphology of NiCoCrAlY-coated René 80 was insignificant after oxidation because the specimen was removed from the test right after the crossover (500 h). Scale spallation occurred on NiCoCrAlY-coated CMSX-4 after 1250 h. Also, some spallation was observed on the NiAl coating after 1000 h despite the extremely low mass gain.

As indicated in Fig. 10, the coating cross-sections after exposure exhibited rougher coating surfaces for the electro-codeposited NiCoCrAlY coatings, as compared to the NiAl coating. According to the EDS analysis, a mixture of Al_2O_3 and spinel oxides was formed on NiCoCrAlY-coated René 80. Less spinel was formed on NiCoCrAlY-coated CMSX-4, whereas cracking was observed in the oxide scale. For NiAl-coated René 80, the Al_2O_3 scale was relatively flat and spallation could also be seen on the cross-section. Interdiffusion between the NiAl coating and the superalloy substrate led to the formation of the precipitates rich in refractory metals underneath the coating interdiffusion zone. Some Ti/Cr-rich particles were also found in the substrate. In contrast, no such precipitation was observed in the NiCoCrAlY-coated samples after thermal exposure. The absence of the precipitation zone is a real advantage in maintaining mechanical integrity of coated superalloys, especially for thin-walled turbine components, due to the brittle nature of these precipitates.

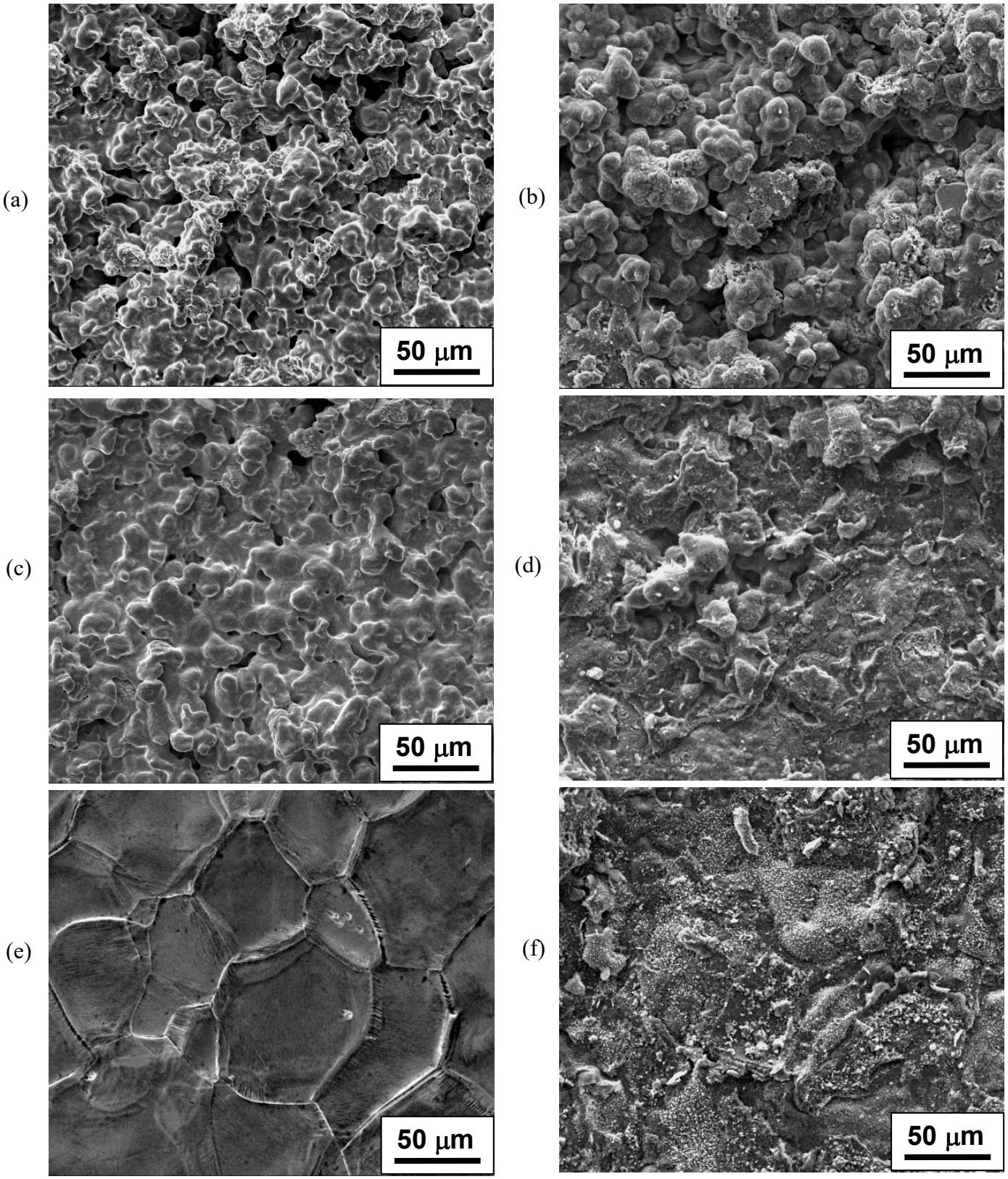

Fig. 9. SEM secondary-electron plan view images of selective coatings before and after cyclic oxidation at 1100 °C: NiCoCrAlY coating on René 80 before (a) and after 500 h (b); NiCoCrAlY on CMSX-4 before (c) and after 1250 h (d); non-contact pack NiAl coating on René 80 before (e) and after 1000 h (f). Both electro-codeposited coatings were 100 μm thick and were heat-treated at 1080 °C in vacuum.

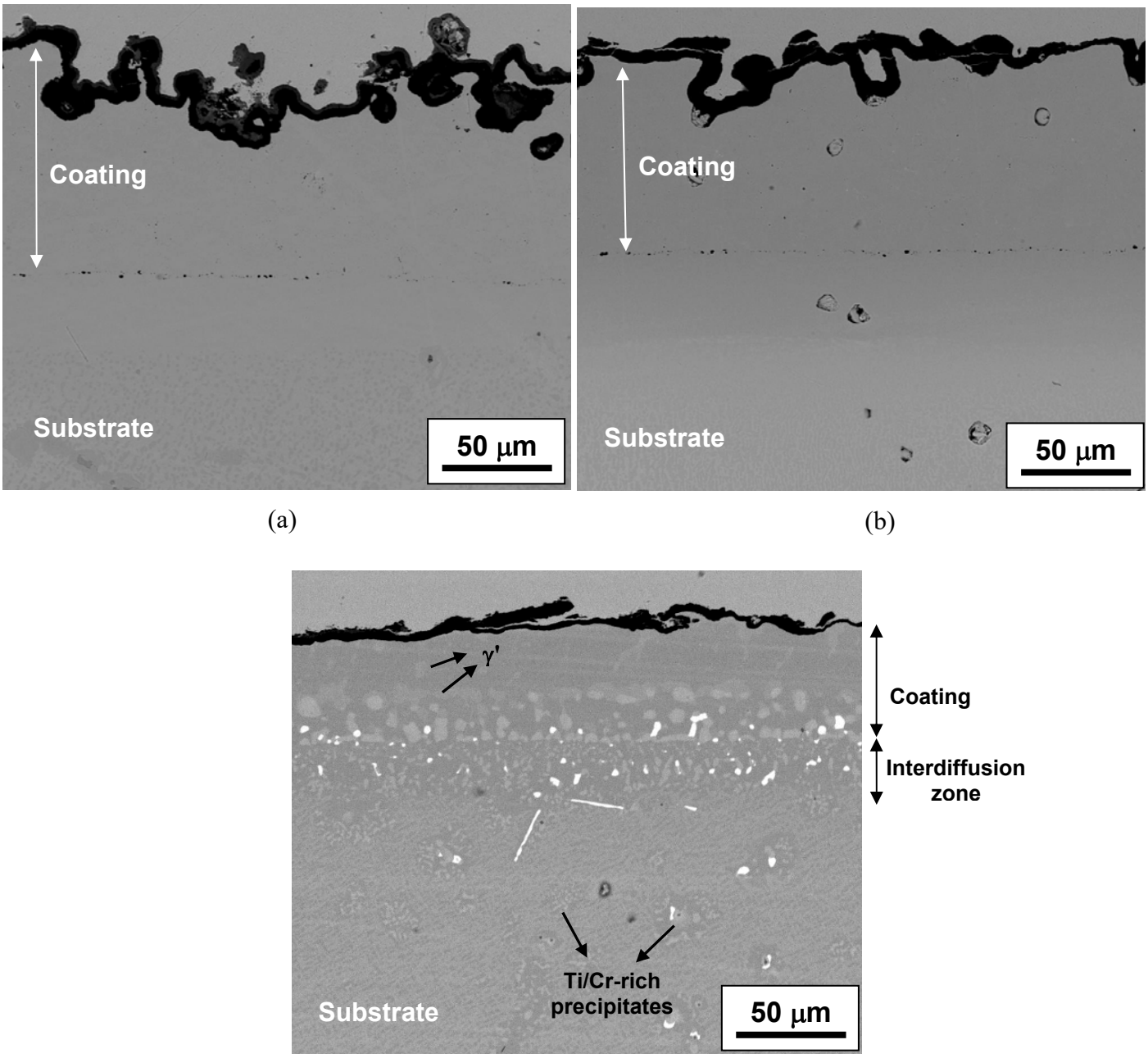

Fig. 10. SEM backscattered-electron images of the cross-sections of coated superalloy specimens after cyclic oxidation at 1100 °C: (a) NiCoCrAlY coating on René 80 after 500 h; (b) NiCoCrAlY on CMSX-4 after 1250 h; (c) non-contact pack NiAl coating on René 80 after 1000 h. Both electro-codeposited coatings were 100 μm thick and were heat-treated at 1080 °C in vacuum.

3.3. Evaluation of the hot corrosion performance of MCrAlX coatings

Bare and coated superalloy specimens and several model NiCoCrAlY cast alloys (as listed in Table 3) were tested in a Dean rig under Type I hot corrosion condition for 20 to 200h. Figure 11 shows the microstructures of uncoated and coated specimens after the corrosion tests. Uncoated

René 80 exhibited better hot corrosion resistance than uncoated René 142, which was attributed to the higher Cr content in the alloy (14.1 vs. 6.7 wt.%). Although the NiAl coating showed good oxidation resistance, it was extensively attacked after only 20h in the hot corrosion test, due to the low Cr solubility in the β-NiAl coating. On the other hand, the electrodeposited NiCoCrAlY coating exhibited superior corrosion resistance over the 100h test, as compared to the diffusion coatings.

Table 3. Corrosion tested specimens.

Sample ID	**Description**	**Testing Duration (h)**
René 80	Uncoated René 80, polished	100
René 80 Grit	Uncoated René 80, grit-blasted	40
René 80 G&S	Uncoated René 80, one side grit-blasted & one side polished	100
René 142	Uncoated René 142, polished	100
René 142 Grit	Uncoated René 142, grit-blasted	100
Alloy NiCrAlY	Ni-31Cr-11.25Al-0.65Y model alloy, polished	200
Alloy NiCrAlY Grit	Ni-31Cr-11.25Al-0.65Y model alloy, grit-blasted	200
Alloy NiCoCrAlY	Ni-12Co-18Cr-12Al-0.5Y model alloy, polished	100
Alloy NiCoCrAlY Grit	Ni-12Co-18Cr-12Al-0.5Y model alloy, grit-blasted	100
BNC-HT	Electrodeposited MCrAlY coating, heat-treated in vacuum	100
BNC-ARF	Electrodeposited MCrAlY coating, heat-treated in Ar	100
NiAl-1	Non-contact pack NiAl coating	40
NiAl-2	Non-contact pack NiAl coating	20

A statistical approach was used to evaluate the hot corrosion data, and a normal distribution was assumed. The cumulative distribution function (CDF) was obtained by first arranging the data in order of magnitude and then at each point determining the probability of a given depth of corrosive penetration using:[16]

$$P(x_i) = \frac{number\ of\ \ observations < x_i}{n+1}$$ for corrosion less than a given value, or

$$Q(x_i) = \frac{number\ of\ \ observations \geq x_i}{n+1}$$ for corrosion greater than or equal to a given value.

The probability plots of uncoated and coated René 80 specimens are shown in Fig. 12. Use of these probability plots is particularly valuable when assessing the behavior of coatings since it is easy to extrapolate to find the likelihood of complete loss of a coating.[16] Based on the assessment of the probability plots, the rank of corrosion resistance from high to low is as

follows: electrodeposited NiCoCrAlY heat-treated in vacuum, uncoated René 80 substrate, NiCoCrAlY heat-treated in Ar, and the NiAl coating.

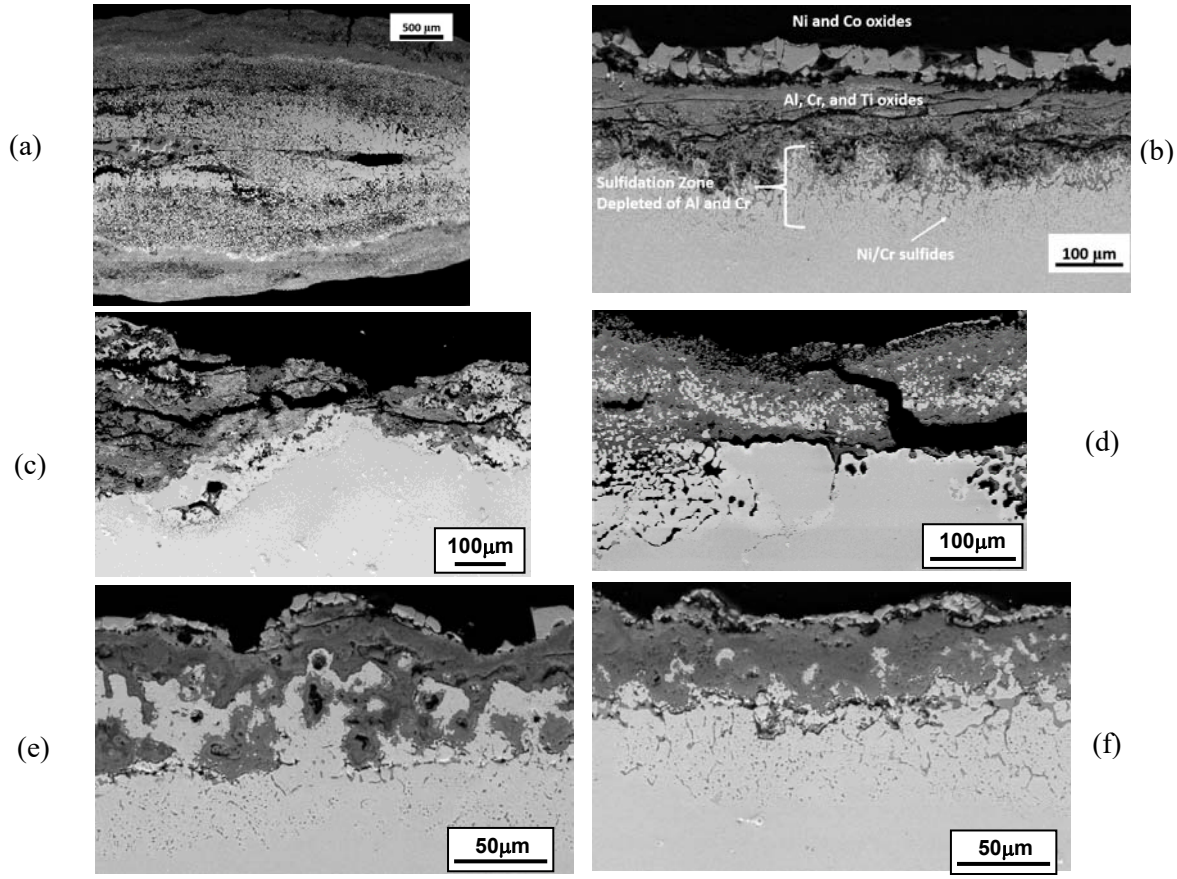

Fig. 11. Cross-sectional microstructure after Type I hot corrosion: (a) uncoated René 142 (100h), (b) uncoated René 80 (100h), (c) NiAl-1 (40h), (d) NiAl-2 (20h), (e) BNC-HT (100h), and (f) BNC-ARF (100h).

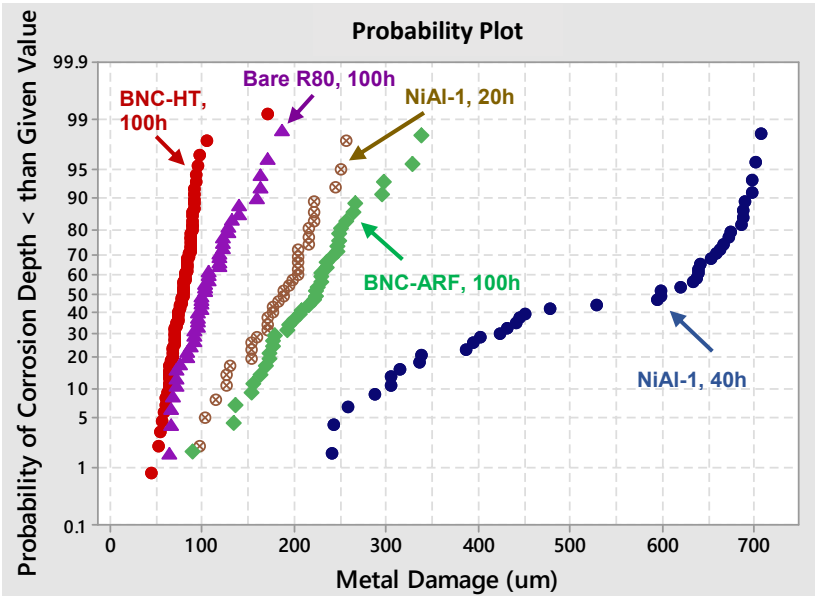

Fig. 12. Probability plots of uncoated and coated René 80 specimens.

3.4. Investigation of the mechanical properties of MCrAlY model alloys

To understand the effect of the coating composition (particularly the Al and Cr levels) on its mechanical properties,[17-20] a group of MCrAlY model alloys (Table 4) were evaluated in tensile testing in a temperature range of 20-800°C. The alloy compositions were chosen to simulate our current coating composition or to represent coatings/alloys that had been reported in the literature with promising oxidation/hot corrosion resistance.

Table 4. Model alloy compositions (in wt.% and at.%).

ID		Ni	Co	Cr	Al	Y	Cr/Al	Notes
#1	wt.%	**60.4**	**15.0**	**14.0**	**10.0**	**0.6**	**1.4**	Close to our baseline coating composition
	at.%	53.3	13.2	14.0	19.2	0.3	0.7	
#2	wt.%	**49.4**	**20.0**	**18.0**	**12.0**	**0.6**	**1.5**	Representative of typical MCrAlY coating compositions
	at.%	42.5	17.2	17.5	22.5	0.3	0.8	
#3	wt.%	**41.4**	**20.0**	**26.0**	**12.0**	**0.6**	**2.2**	Cr level similar to BC23 [21]
	at.%	35.3	17.0	25.1	22.3	0.3	1.1	
#4	wt.%	**36.6**	**20.0**	**31.0**	**12.0**	**0.6**	**2.5**	Cr/Al similar to Taylor & Task's alloys [22,23] but containing Co
	at.%	31.0	16.9	29.7	22.1	0.3	1.3	
#5	wt.%	**36.7**	**22.0**	**35.0**	**6.0**	**0.2**	**5.6**	Similar to Gleeson's high Cr low Al alloy [24]
	at.%	33.0	19.7	35.5	11.7	0.1	2.9	
#6	wt.%	**60.4**	**15.0**	**14.0**	**10.0**	**0.6**	**1.4**	Repeat #1 to check cracks
	at.%	53.3	13.2	14.0	19.2	0.3	0.7	
#7	wt.%	**47.4**	**20.0**	**22.0**	**10.0**	**0.6**	**2.2**	Cr level between #2 (18Cr) and #3 (26Cr)
	at.%	41.5	17.4	21.7	19.0	0.4	1.1	
#8	wt.%	**36.7**	**22.4**	**34.6**	**6.2**	**0.2**	**5.6**	Repeat #5, higher heat treatment temperature (1300°C/4 h)
	at.%	32.9	20.0	35.0	12.0	0.1	2.9	
#9	wt.%	**53.4**	**22.0**	**14.0**	**10.0**	**0.6**	**1.4**	Similar to #1 with higher Co content (1300°C/4 h)
	at.%	47.1	19.4	14.0	19.2	0.4	0.7	

Among the alloys tested, only three alloys showed limited ductility at room temperature, i.e., 18Cr-20Co-12Al, 22Cr-20Co-12Al, and 35Cr-22Co-6Al (wt.%), as shown in Fig. 13. Other alloys fractured during elastic loading and the yield strength and ultimate tensile strength could not be estimated. Some of the high-Cr specimens (31Cr and 35Cr) also exhibited cracks after casting. Figure 14 shows the tensile properties as a function of temperature for the three promising model alloys. Overall, the alloys showed very low ductility up to 400°C (Fig. 14c), which was as expected since the ductile-to-brittle transition temperature (DBTT) for these alloys are around 700°C. Better ductility was observed for the two alloys containing 18Cr and 22Cr.

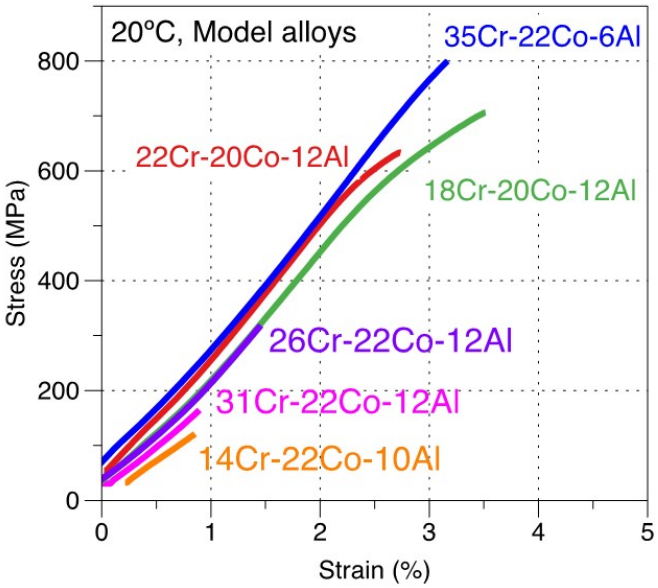

Fig. 13. Stress-strain curves of the model MCrAlY alloys at 20°C.

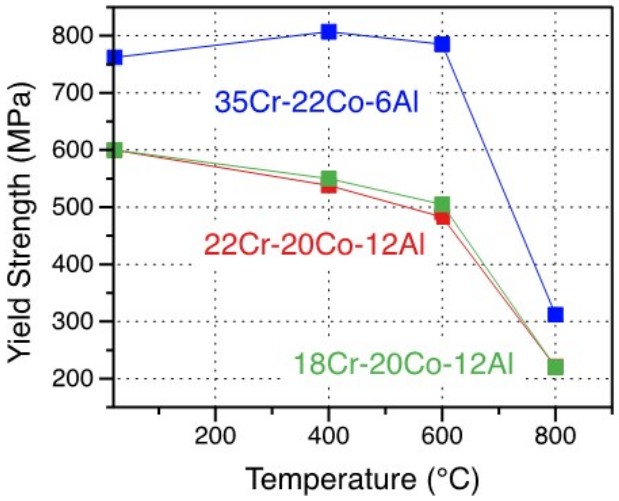

(a)

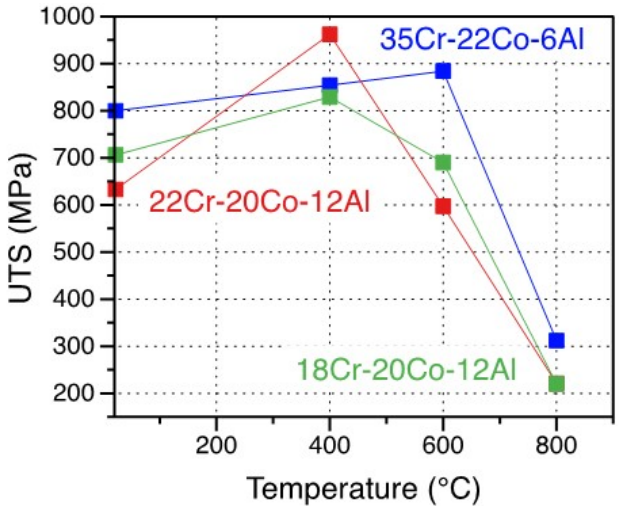

(b)

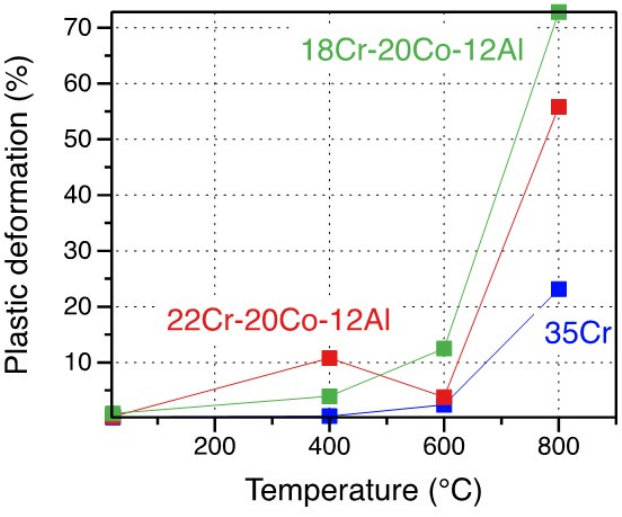

(c)

Fig. 14. Tensile properties of the model MCrAlY alloys at 20-800°C: (a) yield strength, (b) ultimate tensile strength (UTS), and (c) ductility.

Vickers tests were initially carried out on the polished cross sections using a load of 200 gf. Hardness of several alloys was re-evaluated using a load of 500 gf, and similar results were obtained. Each hardness value was taken as the average of at least five measurements. In general, the alloys with < 26 Cr showed similar hardness values (~370 HV), which increased to ~700 HV for the 31Cr alloy (Fig. 15). However, for the 35Cr alloy a drop of hardness to 480 HV was observed, which was likely due to the lower percentage of β phase in the alloy as compared to other high-Cr alloys. Similar hardness values were obtained for both 35Cr alloys, regardless of the heat treatment temperature (1000 or 1300°C). XRD (Fig. 16) and SEM microstructural analyses confirmed the presence of σ and α-Cr phases in the higher Cr alloys (≥26Cr). Also, the amount of β phase was low in the 35Cr alloy.

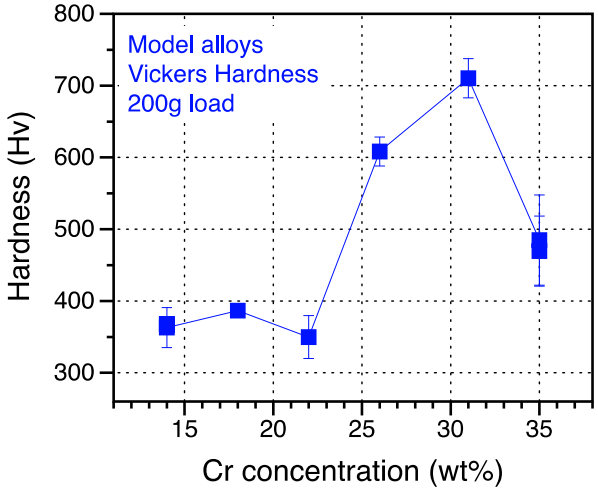

Fig. 15. Microhardness of model MCrAlY alloys as a function of Cr content.

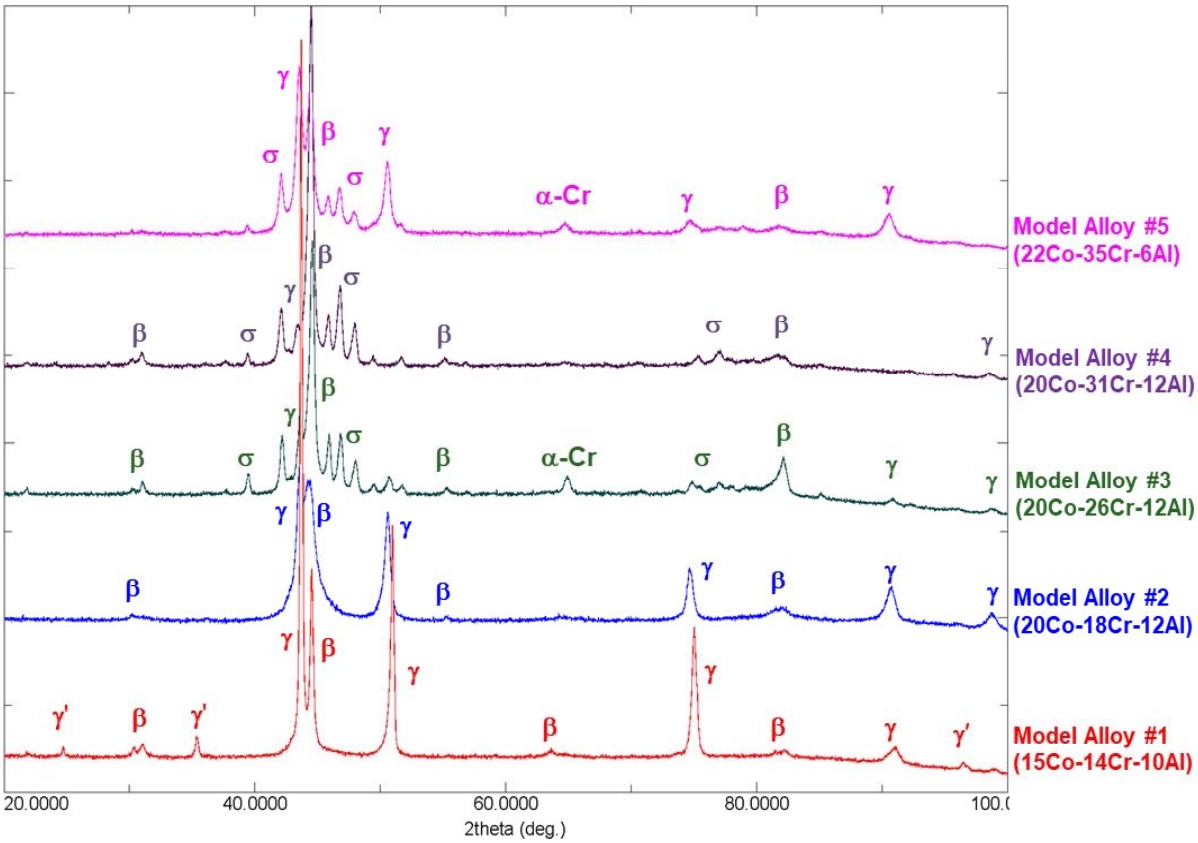

Fig. 16. XRD patterns of the model MCrAlY alloys.

3.5. Development of MCrAlX coatings on burner rig pins

Based on the promising testing results for the coupon samples, the electrodeposited MCrAlX coatings were later applied on the burner rig specimens.

Burner rig samples are typically cylindrical pins, 1/8" (3.2 mm) in diameter and 2½-3" (63.5-76.2 mm) long. The size of our original rotating barrel was 52 mm (ID) x 70 mm (length). To accommodate the burner rig pins, longer barrels with a reduced diameter were needed. Different barrel configurations were designed and several prototype versions were made using 3D printing. However, typical materials (such as ABS or nylon) used in 3D printing do not have adequate long-term corrosion resistance for the Ni-Co plating solution. After testing of 3D-printed prototype barrels, the best barrel configuration was selected and a new barrel made of polypropylene frame was machined at a local machine shop and assembled in our lab.

To identify the optimal electro-codeposition parameters for the burner rig pins, several 1/8"-diameter dummy samples were plated using the parameters previously used for the disc samples in a plating solution containing TTU's ball-milled CrAlY powder. However, the resultant particle incorporation was 25-29 vol.%, which was lower than what had been obtained on the disc samples or larger diameter rods (35-40 vol.%). In order to determine whether the small diameter (curvature) contributed to the lower particle incorporation, stepped stainless steel dummy samples (as shown in Fig. 17) with three different diameters were prepared and coated using both TTU's CrAlY powder and Sandvik's gas-atomized 5-μm CrAlY powder. It was noticed that when the concentration of CrAlY particles in the solution was high enough (100-140 g/L), the specimen curvature did not seem to affect the particle incorporation in the electro-codeposited coating, and ~35 vol.% particle incorporation was achieved.

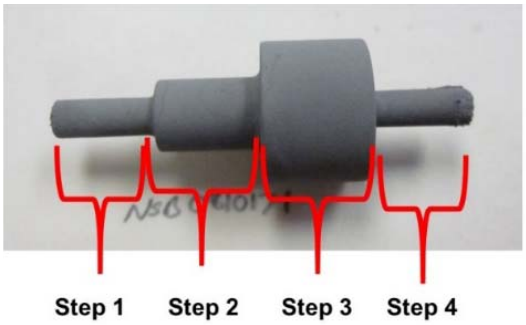

Fig. 17. Image of the stepped specimen.

Since it was difficult to obtain sufficient powder with our powder making process (arc melting − ball milling − sieving) to coat the burner rig pins, we contacted powder manufacturing companies (more than ten powder suppliers) to procure the CrAlY-based powders. Approximately 5 kg of gas-atomized CrAlY powders (d_{50} = 10 μm) was purchased from Sandvik. Some 3" dummy pins were first coated using this powder. Figure 18 shows the as-deposited cross-section of the coated dummy pin and the microstructure after vacuum heat treatment at 1080°C. Table 5 summarizes the particle incorporation measured at three locations (Fig. 19) in the coated dummy pins. With Sandvik's powder, satisfactory particle incorporation with an average value of ~45 vol.% was achieved. The difference in particle distribution along the length of the pin was very small.

In addition, special fixtures for post-deposition heat treatment were designed which were able to hold two burner rig pins for each run. Six burner rig pins were coated in the rotating barrel and heat-treated under vacuum at 1080°C for 6h. The coated pins are being tested under Type I and Type II hot corrosion conditions in the burner rigs at ONR-designated facilities.

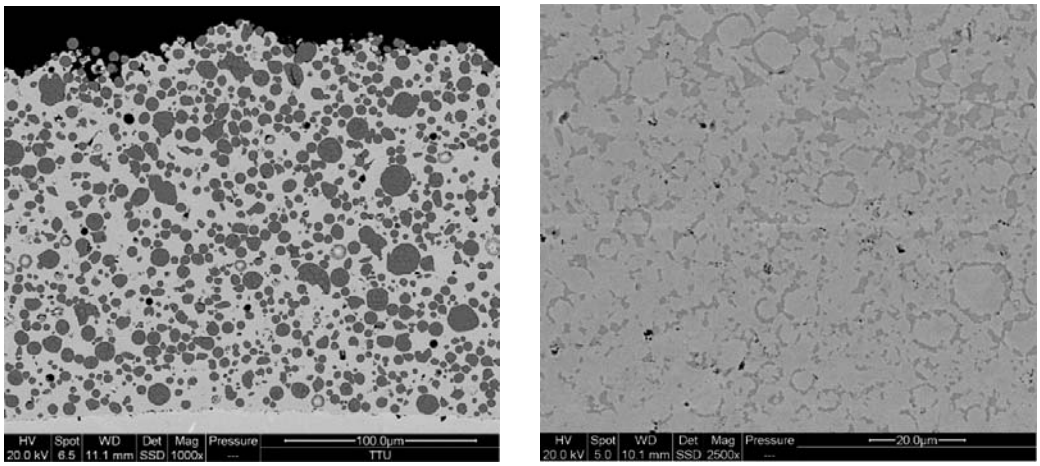

(a) (b)

Fig. 18. SEM backscattered-electron images of the cross-sections of coated dummy pins before and after heat treatment (6 h at 1080°C in vacuum).

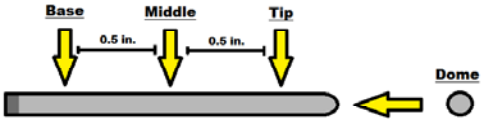

Fig. 19. Schematic showing locations of the particle incorporation measurements.

Table 5. Particle incorporation (vol.%) in coated dummy pins using Sandvik's CrAlY powder.

Location	Base	Middle	Tip
Area 2	45.0	45.1	49.3
Area 3	46.5	43.7	45.8
Area 4	46.5	46.9	46.7
Average	**46.4**	**44.8**	**47.3**

4. Students Supported

Students directly supported by this grant:

- Undergraduate research assistants: Megan Rawls and Giovanni Mainardi
- MS student: Jason Steward (Current Employer: *Y-12 National Security Complex*, Oak Ridge, TN)

– Ph.D. student: Jason Witman (Graduated in December 2018, will start to work at *Arnold Engineering Development Complex*, Arnold Air Force Base, Tullahoma, TN)

Students supported by TTU to assist in this research effort:

– MS student: Giovanni Mainardi

5. Publications

– Y. Zhang, B.L. Bates, J.R. Steward, and S. Dryepondt, "Oxidation and Hot Corrosion Performance of NiCoCrAlY Coatings Fabricated via Electrolytic Codeposition," Oxidation of Metals, online September 2018, DOI https://doi.org/10.1007/s11085-018-9868-z.

– J.C. Witman, "Development and Evaluation of Electro-codeposited MCrAlY Overlay Coatings," PhD Dissertation, Tennessee Tech University, December 2018.

– L.Z. Zhang, B.L. Bates, and Y. Zhang, "Effect of post-deposition heat treatment on electrodeposited NiCoCrAlY coatings," Surface Engineering, 33 (2017) 136-141.

– J.R. Steward, "Hot Corrosion Testing of Ni-Based Alloys and Coatings in a Modified Dean Rig," MS Thesis, Tennessee Tech University, August 2016.

– Y. Zhang, "Electrodeposited MCrAlY Coatings for Gas Turbine Engine Applications," JOM, 67, 2599-2607 (2015).

6. Presentations

– Ying Zhang, Brian Bates, Jason Witman, and Sebastien Dryepondt, "Electrodeposited MCrAlY Coatings for Gas Turbine Engine Applications," MS&T 18, Columbus, OH, October 15, 2018.

– Ying Zhang, Jason Witman, "Electrodeposition of MCrAlY Coatings for Gas Turbine Engine Applications," NASF SUR/FIN 2018, Cleveland, OH, June 4, 2018.

– Ying Zhang (Invited), "Electrodeposited MCrAlY Coatings for Gas Turbine Engine Applications," TMS-Energy Materials 2017, San Diego, CA, February 27, 2017.

– Ying Zhang, Brian Bates, Jason Witman, Jason Steward, Sebastien Dryepondt, and Bruce Pint, "Oxidation and Hot Corrosion Performance of Electrodeposited MCrAlY Coatings," MS&T 16, Salt Lake City, UT, October 27, 2016.

References

[1] D.A. Shifler, "Future research directions to understanding factors influencing advanced high temperature materials", Department of Defense Corrosion Conference, August 10-14, 2009, Washington DC.

[2] B.L. Bates, L.Z. Zhang, and Y. Zhang. "Electrodeposition of Ni matrix composite coatings with embedded CrAlY particles", Surf. Eng., 31 (2015) 202.

[3] B.L. Bates, J.C. Witman, and Y. Zhang, "Electrolytic co-deposition of Ni-CrAlY composite coatings using different deposition configurations," Mater. Manuf. Process., 31 (2016) 1232.

[4] F.J. Honey, E.C. Kedward, and V. Wride, "The development of electrodeposits for high-temperature oxidation/corrosion resistance," J. Vac. Sci. Technol., A 4 (1986) 2593.

[5] J. Foster, B.P. Cameron, and J.A. Carew, "The production of multi-component alloy coatings by particle codeposition," Trans. Inst. Met. Finish, 63 (1985) 115.

[6] Y. Zhang, B.L. Bates, J.R. Steward, and S. Dryepondt, "Oxidation and hot corrosion performance of NiCoCrAlY coatings fabricated via electrolytic codeposition," Oxid. Met., (DOI https://doi.org/10.1007/s11085-018-9868-z), online September 2018.

[7] A.V. Dean, "Investigation into the resistance of various nickel and cobalt base alloys to sea-salt corrosion at elevated temperatures," National Gas Turbine Establishment Report, No. R. 267, 1965.

[8] V. Deodeshmukh and B. Gleeson, "Hot corrosion behavior of Co-and Ni-based aluminide coatings," Corros., 509 (2006) 1.

[9] C.A. Schneider, W.S. Rasband, and K.W. Eliceiri, "NIH Image to ImageJ: 25 years of image analysis," Nature Methods, 9 (2012) 671.

[10] L.Z. Zhang, B.L. Bates, and Y. Zhang, "Effect of post-deposition heat treatment on electrodeposited NiCoCrAlY coatings," Surf. Eng., 33 (2017) 136.

[11] T.J. Nijdam, L.P.H. Jeurgens, J.H. Chen, and W.G. Sloof, "On the microstructure of the initial oxide grown by controlled annealing and oxidation on a NiCoCrAlY bond coating," Oxid. Met., 64 (2005) 355.

[12] I. Keller, D. Naumenko, W.J. Quadakkers, R. Vaßen, and L. Singheiser, "Influence of vacuum heat treatment parameters on the surface composition of MCrAlY coatings," Surf. Coat. Technol. 215 (2013) 24.

[13] A.V. Put, M.-C. Lafont, D. Oquab, A. Raffaitin, and D. Monceau, "Effect of modification by Pt and manufacturing processes on the microstructure of two NiCoCrAlYTa bond coatings intended for thermal barrier system applications," Surf. Coat. Technol., 205 (2010) 717

[14] M.S. Priest and Y. Zhang, "Synthesis of clean aluminide coatings on Ni-based superalloys via a modified pack cementation process," Mater. Corros., 66 (2015) 1111.

[15] B.M. Warnes, "Improved aluminide/MCrAlX coating systems for super alloys using CVD low activity aluminizing," Surf. Coat. Technol., 163 (2003)106

[16] S.R.J. Saunders and J.R. Nicholls, "Hot salt corrosion test procedures and coating evaluation," Thin Solid Films, 119 (1984) 247.

[17] M.I. Wood, "Mechanical properties of coatings and coated systems," Mater. Sci. Eng. A120 (1989) 633.

[18] T.A. Taylor and D.F. Bettridge, "Development of alloyed and dispersion-strengthened MCrAlY coatings," Surf. Coat. Technol., 86-87 (1996) 9.

[19] R.W. Smith, "Mechanical properties of a low-pressure-plasma-applied Co-Cr-Al-Y coating," Thin Solid Films, 84 (1981) 59.

[20] G.W. Meetham, “Use of protective coatings in aero gas turbine engines,” Mater. Sci. Technol., 2 (1984) 290.

[21] D.J. Wortman, “Performance comparison of plasma spray and physical vapor deposition BC23 coatings in the LM2500,” J. Vac. Sci. Technol., A3 (1985) 2532.

[22] T.A. Taylor and P.N. Walsh, “Dilatometer studies of NiCrAlY coatings,” Surf. Coat. Technol., 188-189 (2004) 41.

[23] M.N. Task, “The effect of composition and microstructure on the reaction behavior of MCrAlY alloys under a variety of aggressive environmental conditions,” MS Thesis, University of Pittsburgh, 2009.

[24] B. Gleeson, M. Yanar, G.H. Meier, and F.S. Pettit, “Degradation of TBC systems in environments relevant to advanced gas turbines for IGCC systems,” 2012 University Turbine Systems Research Workshop, Irvine, CA, October 2-4, 2012, http://www.netl.doe.gov/publications/proceedings/12/utsr/index.html.